Supporting Information

Cobalt-plasma treatment enables structural reconstruction of $CoO_x/BiVO_4$ composite for efficient photoelectrochemical water splitting

*Zhongyuan Liu[a], Xiaofeng Wu[a], Beining Zheng[a], Yu Sun[b], Changmin Hou[a], Jie Wu[a], Keke Huang[a] and Shouhua Feng[a]**

Detailed Experimental Section:

The Film Fabrication and Characterization.

High quality epitaxial thin film of $BiVO_4$ were fabricated by pulsed laser deposition (PLD) on FTO substrates. A total of 3000 pules of $BiVO_4$ was deposited at a pulse frequency of 6 Hz and 350 ℃ under 300 mTorr O_2 using a pure $BiVO_4$ target. Then a total of 10000 pules of cobalt were deposited at $5*10^{-6}$ Torr under 50℃, 200℃, 350℃, 500℃, respectively for different samples. A pure cobalt metal target was used during the fabrication.

Electrochemical Measurements.

The current-voltage (I-V) characteristic curves were obtained from a sweeping current-potentiometric scans (LSV) using CHI660E electrochemical workstation (CH Instruments Ins, America). The measurements were performed using a three electrodes system in 0.5M KPi buffered solution (PH ≈ 7.0) under simulated sunlight illumination (AM 1.5G, 100 mW cm-2). LSV data is collected at a scan rate of 10 mV/s. A platinum electrode was used as a counter electrode. As the potential was reported against the reversible hydrogen electrode (RHE) a silver chloride electrode (Ag/ AgCl) was used as a reference electrode:

$E_{RHE} = E_{AgCl} + 0.059pH + E^0_{AgCl}$, with $E^0_{AgCl} = 0.1976$ V at 25℃. (1)

Electrochemical impedance spectroscopy measurements (EIS), Current-time curves, were performed using a CHI660E electrochemical workstation (CH Instruments Ins, America). The measurements were performed at room temperature at 1.23 $V_{RHE.}$

Current-time curves were performed at room temperature at 1.23 $V_{RHE.}$

OCPT were performed at

The PEC sulfite photooxidation uses 0.5 M Na_2SO_3 as the hole scavenger.

Charge transfer ($\eta_{transfer}$) efficiencies which could also be referred to the charge injection efficiencies were calculated using the following equations:

$$\eta_{transfer} = \frac{J_{H_2O}}{J_{Na_2SO_3}}$$

where JH_2O and JNa_2SO_3 represent the measured photocurrent densities in water oxidation in the presence or absence of a hole scavenger (Na_2SO_3), respectively. Na_2SO_3 was used as a hole scavenger during oxidation because of its higher kinetic speed compared to water, which makes its charge transfer efficiency ~ 100 %. In addition, the incident photon-to-current conversion efficiency (IPCE) was measured with simulated sunlight illumination (AM 1.5G, 100 mW cm^{-2}). equipped with optical filters on 400, 420, 450, 475, 500, 520 and 550 nm. IPCE was calculated using the following equation:

$$\text{IPCE}\ (\%) = \frac{J_{ph(\lambda)}}{P_{\text{light}}} \times 1240\lambda(\text{nm}) \times 100$$

where Jph is the photocurrent density, P_{light} is the power density, and λ is the wavelength.

Material characterization

X-ray diffraction (XRD) characterization was conducted on a D8 Venture (Bruker, Germany). Scanning electron microscope (SEM) images, Energy-dispersive X-ray spectroscopy (EDS) mapping images were acquired on Helios NanoLab 600i (FEI, USA). High-resolution transmission electron microscopy (HRTEM) and Energy-dispersive X-ray spectroscopy (EDAX)were acquired on a Tecnai G2 F20 S-Twin electron microscope (FEI, USA). X-ray photoelectron spectroscopy (XPS) was performed on VG EXCALAB 210 with Al Kα radiation (Thermo, USA)

DFT calculation

First-principles DFT calculations were performed by using the Vienna ab initio Simulation Package (VASP) in our work. The projector-augmented wave (PAW) potentials were used to describe the electron−ion interactions and the electron exchange-correction function was described by the generalized gradient approximation (GGA) parametrized by Perdew−Burke−Ernzerhof (PBE). The cutoff energy was set to 500 eV. The atomic positions were fully optimized until the forces on the atoms are below 0.05 eV/Å. The convergence threshold for self-consistent-field (SCF) iteration was set at 10−6 eV.

Results and Discussion

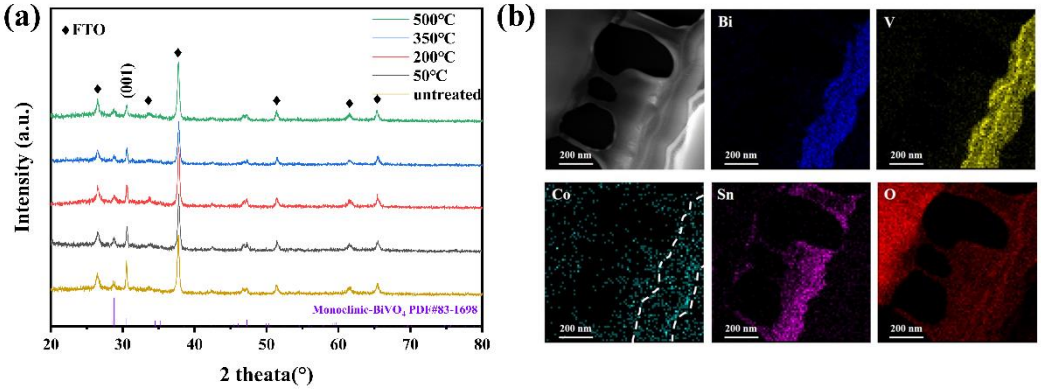

Figure S1. (a) XRD data of samples treated under different crystallization temperatures. (b) Element mapping of samples treated under 200℃.

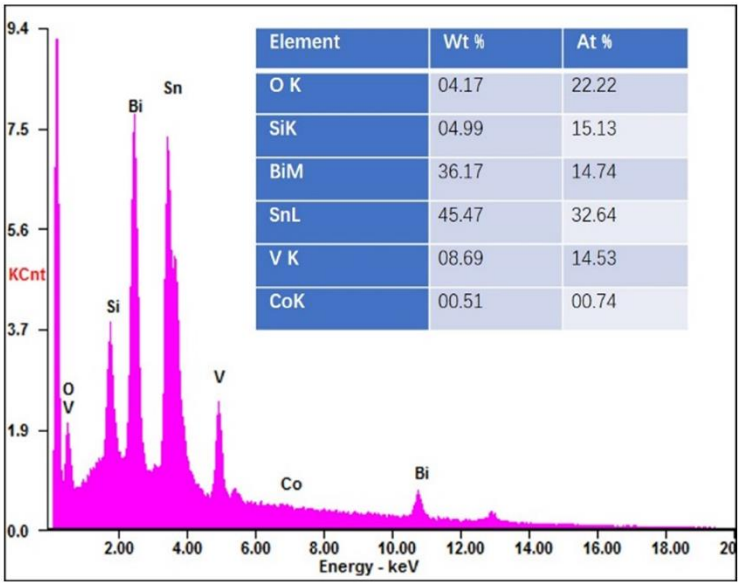

Figure S2 Energy dispersive x-ray analysis (EDAX) of samples treated under 200℃. Inserted table is an elements composition analyst.

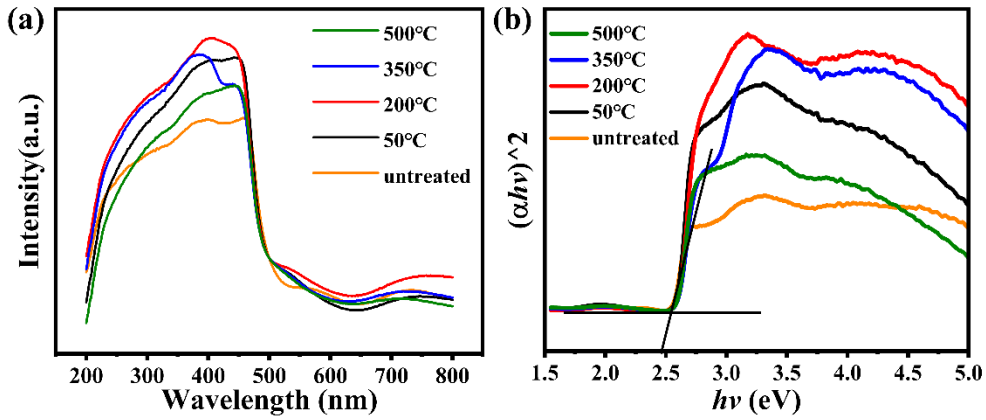

Figure S3 Solid UV-Vis absorption measurement of samples treated under different temperatures.

From this measurement, we can conclude the cobalt could increase the light absorber light absorption capacity, which has been reported before [1].

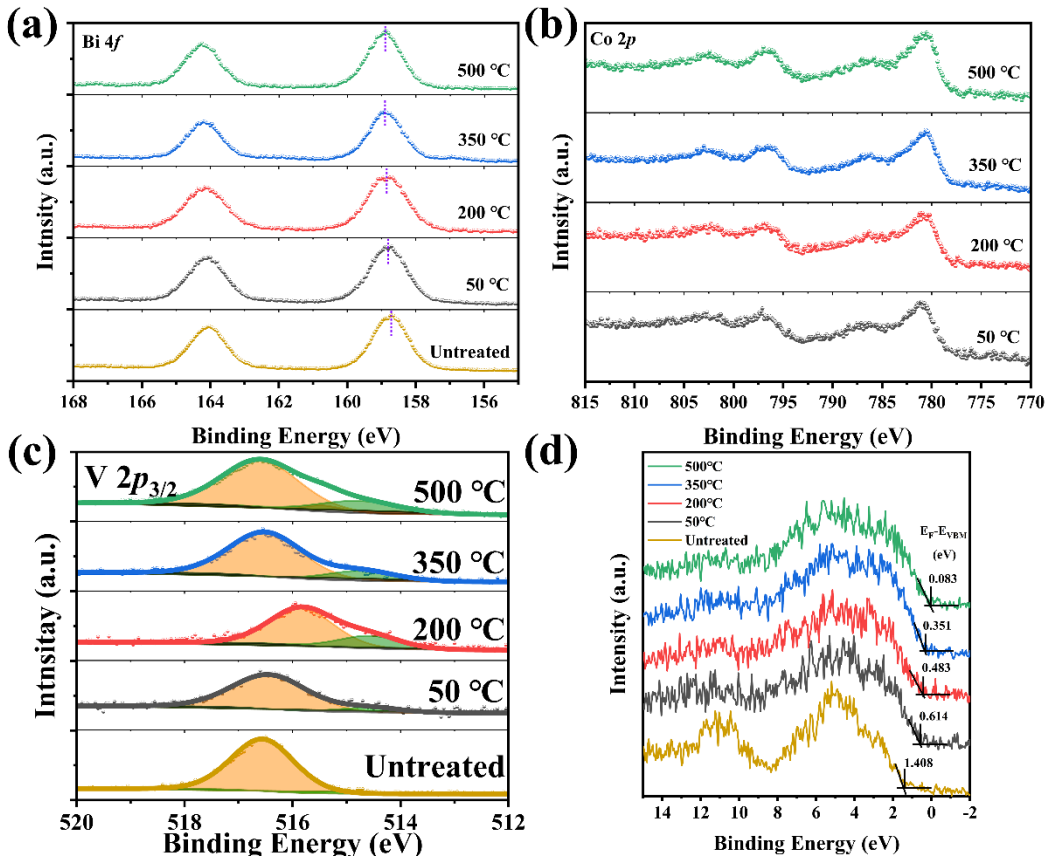

Figure S4. (a) Bi 4*f* of samples treated with cobalt plasma under different temperatures. (b) Co 2*p* of samples treated with cobalt plasma under different temperatures. (c) V $2p_{3/2}$ of samples treated with cobalt plasma under different temperatures. (d) Valance top of samples treated with cobalt plasma under different temperatures.

From the XPS data could find that the Bi is slightly shift to high energy which shows a charge redistribution. Co 2*p* shows the valance is Co^{2+}. V 2*p* indicated the V^{4+} appeared. V^{5+} shifts about 1eV from original position under 200 °C which demonstrate an obviously charge redistribution. Valance top of samples with treatment becomes board. It leads the improvement of surface conductivity. The generation of new energy gap could also broaden the valance top.

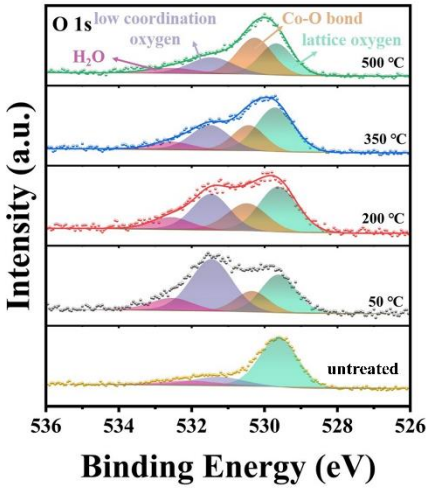

treatment	As is (bare)	50℃	200℃	350℃	500℃
Lattice oxygen	1.00	0.63	1.00	1.00	0.80
Co-O bond	——	0.33	0.60	0.58	1.00
Low coordination oxygen	0.22	1.00	0.75	0.56	0.44
H_2O	0.11	0.23	0.25	0.17	0.14

Figure S5. O 1*s* of samples treated with cobalt plasma under different temperatures. The table lists the composition of different oxygen species of samples treated with cobalt plasma under different temperatures.

According to O 1*s* data, the composition of different oxygen species changes a lot. It reflects the surface chemical are changed through change the processing temperature.

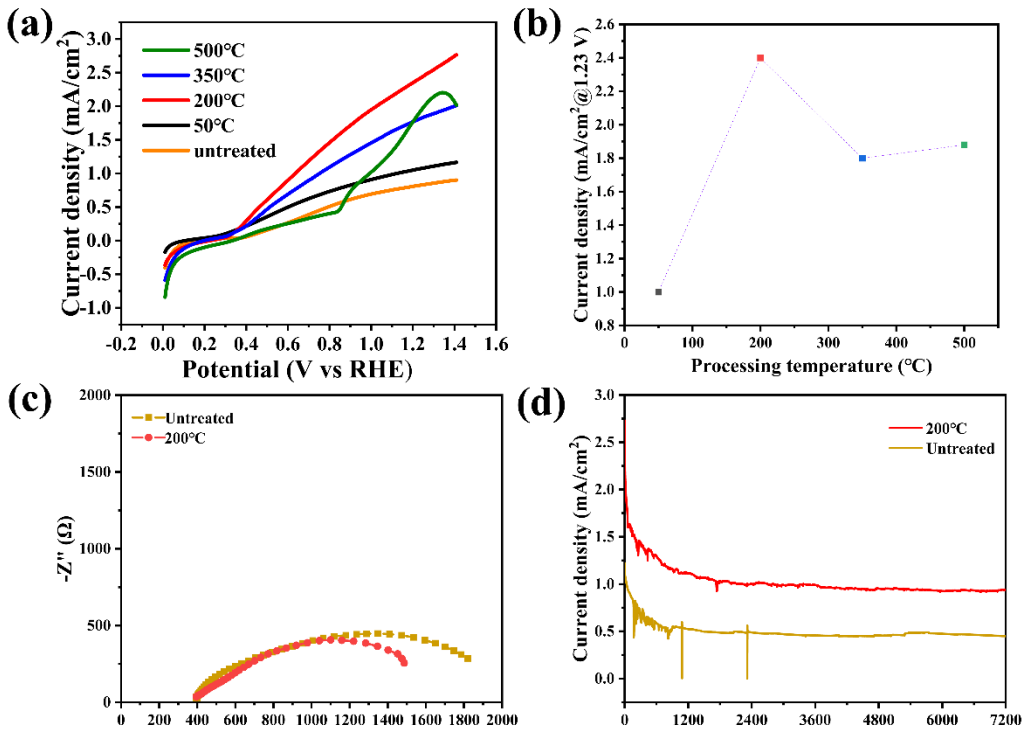

Figure S6. (a) LSV data of samples treated with cobalt plasma under different temperatures. (b) Photocurrent density at 1.23 eV v.s. RHE of samples treated under different temperatures (c) EIS data of samples etched under 200 °C and untreated $BiVO_4$. (c) Photocurrent-time curves for stability measurement of samples etched under 200 °C and untreated $BiVO_4$.

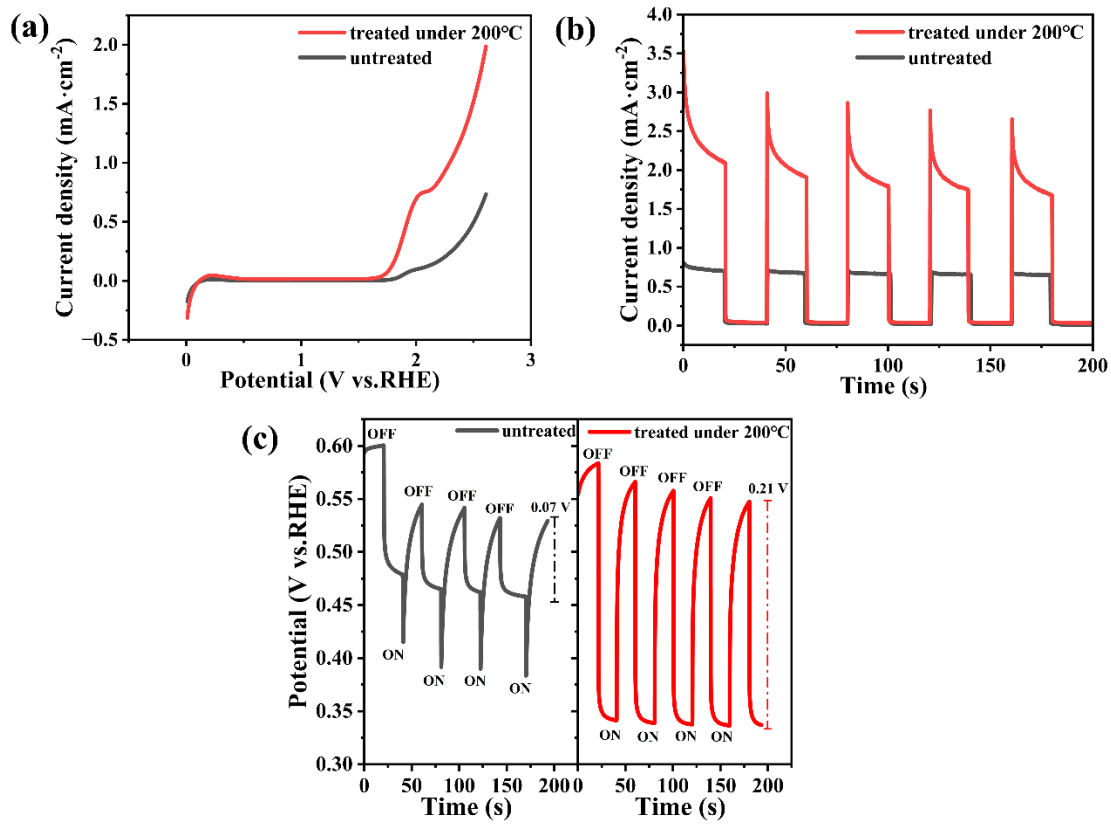

Figure S7 (a). Dark LSV of untreated $BiVO_4$ sample and the one treated with cobalt-plasma under 200 ℃. (b). Current-time curves of untreated BiVO4 sample and the one treated with cobalt-plasma under 200 ℃. (c). Open circuit potential-time curves of untreated BiVO4 sample and the one treated with cobalt-plasma under 200 ℃.

Dark LSV are measured shown in Figure S7 (a). It shows an obvious improvement of water oxidation reaction after the cobalt-plasma treatment. This enhancement of surface water oxidation under dark condition demonstrate that there is a better water oxidation center on the BVO after the treatment. The photocurrent density-time curves are measured shown in Figure S7 (b). There are spikes in these curves indicating the accumulation of photogenerated holes at the surface of photoanode. [2] A larger spike under a higher photocurrent density in the treated sample indicates more holes have been accumulated in the surface of composite photoanode. The Co^{2+}/Co^{3+} as a hole accumulate center prevent the surface recombination of photo-generated carriers successfully.

Further, the open circuit potential (OCP) measurement is used to clarify the difference of photovoltage before and after the treatment shown in Figure S7 (c). The U_{OC} value of $CoO_x/BiVO_4$ is higher than untreated one, which means the treatment could suppressed the surface charge trapping effectively and provide a higher photovoltage for PEC reaction. [3]

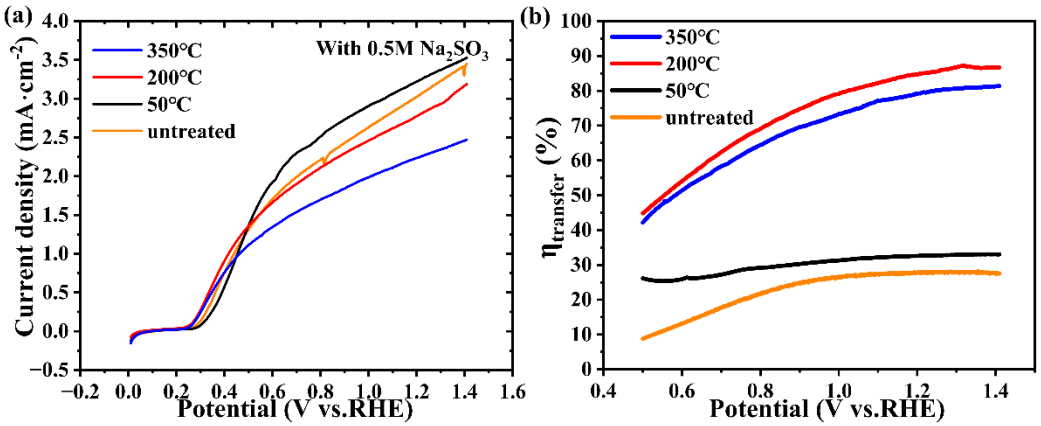

Figure S8 (a). PEC sulfite photooxidation reaction of samples treated under different temperatures. (b) $\eta_{transfer}$ of samples treated under different temperatures.

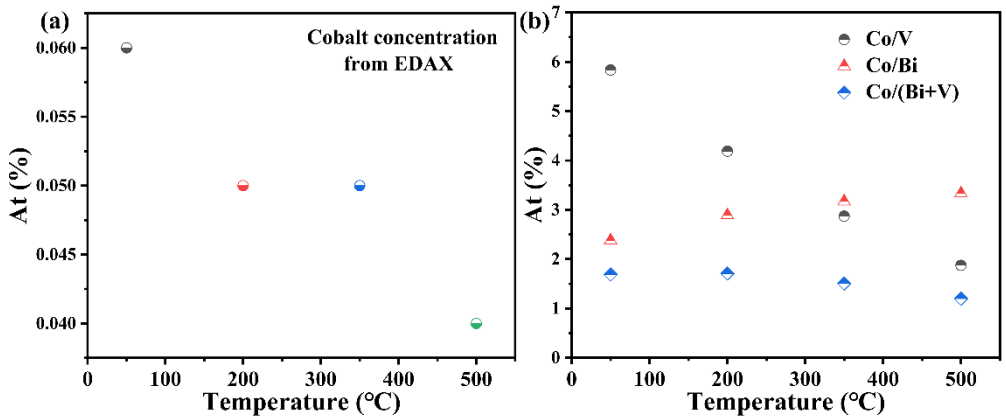

Figure S9 (a) Cobalt concentration in different samples from EDAX data. (b) Elemental composition of different samples.

References:

1. Y Geng, P Zhang, N Li et al., *J. Alloys Compd.*,651 (2015),744-748

2. He B, Zhao F, Yi P, et al., *ACS Appl. Mater. Interfaces*. 2021, 13, 48901-48912.

3. Li Z, Zhang Q, Chen X, et al., *Chem.Commun*. 2020, 56(86), 13153-13156.